

## Modelling and simulation of micropolar fluid flow with variable viscosity through unhealthy artery

J. V. Ramana Reddy<sup>1</sup>, D Srikanth<sup>2\*</sup>

<sup>1</sup> Department of Mathematics, Indian Institute of Technology Madras, Chennai C 600036, India

<sup>2</sup> Department of Applied Mathematics, Defence Institute of Advanced Technology, Pune C 411025, India

(Received May 04 2017, Accepted January 17 2018)

**Abstract.** The article ascertains the physics of the pulsatile two-dimensional blood flow through the flexible tapered artery. The variable dynamic viscosity and variable vortex viscosity are successfully incorporated in the model. To make the model more realistic pulsatile pressure gradient, velocity slip, the permeability of the stenosis and non-vanishing angular momentum at the arterial wall are incorporated in the model. The numerical solution of the transformed governing equations is obtained by using the finite difference method (FDM). The velocity profiles, volumetric flow rate, resistance to the flow and wall shear stress are obtained numerically for various values of fluid and geometric parameters. It is observed that the flow rate is directly proportional to the square of the annular radius and height of the stenosis is highly impact on the physiological dynamics as compared with the catheter radius. Therefore, it is suggested to consider the height of the stenosis while selecting the catheter.

**Keywords:** blood flow, micropolar fluid, variable viscosity, finite difference method

### 1 Introduction

Blood flow in stenosed arteries has been the subject of many studies for the past years and is becoming a very important mean to investigate the cause and development of many cardiovascular diseases. The mathematical model and its numerical simulation can help the investigators for the better understanding of physiological and pathological processes and their correlations. Blood flow results in mechanical and chemical interactions with the vessel walls and tissue, thus giving rise to a complex fluid - structure interaction. Thus, it is a fascinating task for applied mathematicians to represent the working nature of the cardiovascular system in the mathematical form.

The changes in vessel shape due to pathology clearly affect the blood flow. This is due to the mutual interaction between hemodynamic and vascular biology, which is yet to be understood in totality. For example the traction (i.e. the force per unit area) exerted by the flowing blood on the vascular conduit walls directly affects the function of endothelial cell function. The accumulation of excessive fatty components, calcium, erythrocyte aggregation, etc., on the inner wall of the artery results in 'stenosis/constriction'. Medically this situation is referred as 'atherosclerosis'. The obstruction to the blood flow, results in abnormal variations of the blood flow characteristics, thus affecting the functioning of the body parts. Catheterization is a method in which a long skinny versatile tube is inserted into the stenotic artery to treat atherosclerosis. Insertion of such a tube (called catheter) into the lumen of the artery results in significant changes in the blood flow. Therefore, the study of the catheter effects in physiological dynamics through a stenotic artery is vital as studied by Reddy et al. [15]. Recently, Anju et al. [16] considered pulsatile flow of dusty fluid through the axisymmetric stenotic

\* Corresponding author. Tel.: +91 7798229930.

E-mail address: sri\_dasari1977@yahoo.co.in

tube. The time dependent nature of the arterial wall has been considered to understand its effect on blood flow. It is observed that the impact of time on radial velocity is much more than that of the axial velocity.

Srinivastava et al. [20] considered the composite nature of the stenosis in their analysis by believing that, stenosis is caused by the impingement of extra-vascular masses or due to intravascular atherosclerotic plaques which develop at the wall of the artery and protrude into the lumen of the artery. In this article, the increase in impedance has been calculated and understood that the height of the stenosis is strongly responsible for the hype in impedance. The power-law fluid flow through overlapping stenosed arteries was discussed by Ismail et al. [11]. In their investigations, it has noticed that in case of diverging artery, the axial velocity is more in Newtonian models than in the power law model.

The two-dimensional Newtonian rheology of blood flow through tapered arteries without the catheter was studied by Chakravarty et al. [7]. Here the authors used the transformation to get the computational domain and the finite difference method has been applied to simulate the modelled equations.

Noreen Akbar [2] modelled blood as Walter's B fluid. Here author investigated the Walter's B fluid flow through the stenotic tapered artery by the regular perturbation method. The increase in Walter's B fluid parameter makes the fluid thicker thus decrease in velocity, causes decreases in shear stress. It is a well-known fact that, blood is a marvelous fluid with suspension of cells in plasma. While plasma can be considered to be Newtonian in nature, blood has non-Newtonian characteristics, particularly at low shear rates [10]. At a microscopic scale, the orientation of the endothelial cells depends on the wall shear stress induced by the blood. An accurate description of the flow field is thus required to address this type of interaction. The micropolar fluid theory described by Eringen [9] is meant to represent the rheology of the fluids containing rigid randomly oriented particles. These fluids exhibit micro-rotational effects and micro-rotational inertia. Recently Ramana et al. [13] considered a micropolar fluid model to understand the effects of vessel tapering and velocity slip. It is reported that the coupling effects are strongly influencing the impedance, here authors analytically discussed the steady model. Srinivasacharya et al. [18] discussed time dependent effects through a bifurcated artery by considering micropolar fluid. Here examined that increase in the micropolar coupling number leads to enhancement in the resistance to the flow, as reported in [13]. An increase in the value of coupling number leads to an increase in the angular velocity indicating that an increase in vortex viscosity enhances the rotation of the micro-elements. Hence, the microstructure becomes significant in enhancing the impedance. Wu et al. [21] modelled the blood as a mixture of viscous fluid (as plasma) and non-linear fluid with a shear dependent viscosity (for blood components) and analyzed the volume fraction of the RBC's impact on plasma and compared with the experimental data as well. In the present model, the whole blood treated as one unit, and modelled with polar fluid with variable viscosity due to hematocrit.

Blood viscosity is a measurement of the thickness and stickiness of blood. It determines the amount of friction against the blood vessels, the degree to which the heart must work and the quantity of oxygen to be delivered to the tissues and organs. It is a direct measure of the "flow ability" of blood. Blood viscosity is correlated to the major risk factors of cardiovascular diseases like age, volume of red blood cells (RBC), smoking, obesity, inflammation, insulin resistance, high blood pressure and others. Among all the above Hematocrit is the most obvious determinant of Whole Blood Viscosity (WBV). Hematocrit accounts for about 50% of the difference between normal blood viscosity and high blood viscosity. Hence the consideration of Hematocrit is very important in modelling the blood flow phenomena.

Srinivasacharya et al. [19] considered vanishing micro-rotation parameter in their analysis. However, it is understood that, in the neighborhood of the boundary, the rotation is only due to shear and therefore, as given by Ahmadi et al. [1] the gyration vector must be equal to the angular velocity. It is understood that the slip velocity at the arterial wall may form in two ways. Firstly, because of deposition of cholesterol and other fatty substances at the arterial wall. And secondly, because of consideration of the permeable stenosis. The second case was suggested by Beavers [3]. In which they showed that there is net tangential drag due to the transfer of forward momentum across the permeable interface leading to the slip in velocity.

Based on the above literature survey, it is therefore proposed to discuss the effects of variable viscosity in blood flow through flexible tapered stenotic artery with mild stenosis. Blood is characterized by micropolar fluid. Darcy law is used to account for the permeable nature of the stenosis. The highly nonlinear equations are solved using the Finite Difference Method (FDM). The flow quantities such as the axial velocity ( $v$ ), the flow

rate (Q) and the physiological parameters such as the impedance ( $\Lambda$ ) and the shear stress ( $\tau$ ) distribution at the wall of the  $\omega$ -shaped permeable stenotic artery are computed and are discussed for various fluid and geometric parameters.

## 2 Problem formulation

### 2.1 Schematic diagram

Consider the micropolar fluid flow through an  $\omega$ -shaped flexible stenotic tapered artery in the presence of the catheter. The flow is assumed to be fully-developed. Any point in the geometry is represented by the cylindrical polar coordinates  $(r, \theta, z)$ ; where  $r$  quantify in radial direction and that of  $\theta$  and  $z$  designate the circumferential direction and axial direction respectively. The mathematical representation of the  $\omega$ -shaped stenotic flexible tapered artery is considered as given by Reddy et al. [14]

$$h(z, t) = \begin{cases} \left[ r_0 + \zeta z - \frac{3}{2} \frac{\epsilon}{R_0 L_1^4} \left( 11(z - L_0) L_1^3 - 47(z - L_0)^2 L_1^2 \right. \right. \\ \left. \left. + 72(z - L_0)^3 L_1 - 36(z - L_0)^4 \right) \right] f(t), L_0 \leq z \leq L_0 + L_1 \\ \left[ r_0 + \zeta z \right] f(t), \text{ otherwise} \end{cases}$$

where  $f(t)$ , expressed as  $\left[ 1 - b \left( \cos(2\pi f_p t) - 1 \right) e^{-2\pi f_p t b} \right]$  corresponds to the flexible nature of the arterial wall. Here,  $f_p$  corresponds to the pulsatile frequency,  $b$  is an arbitrary constant representing the amplitude of  $f(t)$ ,  $\zeta (= \tan(\phi))$  is the tapering parameter and  $\phi$  is the corresponding tapering angle.  $\phi (> 0$  and  $< 0$ ) corresponds to the diverging and converging nature of the artery, whereas  $\phi (= 0)$  indicates the non-tapered nature of the artery.  $\epsilon$  is the maximum height of the stenosis which protrudes into the lumen of the annular region. The radius of the annular region in case of non-tapered and non-stenotic region is represented by  $r_0$ . The modelled fluid is flowing in an annular region formed by a flexible artery with varying radius  $h(z, t)$  and a catheter of radius  $r_c$ . Here  $z_C$  indicates the location on z-axis corresponding to the critical height of the overlapping stenosis.  $z_L$  and  $z_R$  correspond to the locations where maximum heights of the stenosis are occurring. The annular radii and the extreme height locations for various values the geometric parameters were obtained by Reddy et al. [13].  $L_0$  is the length from left end of the arterial segment up-to the starting of the stenosis and the length of the stenosis is considered as  $L_1$ , as shown in Fig.1.

### 2.2 Blood flow model

The governing equations for the incompressible homogenous micropolar fluid flow in the absence of body forces and body couple are given by

$$\nabla \cdot \vec{V} = 0 \quad (1)$$

$$-\nabla P + 2\nabla \times \left[ k(r) \omega \right] + \nabla^2 \left[ (\mu(r) + k(r)) \vec{V} \right] = \rho \frac{D\vec{V}}{Dt}, \quad (2)$$

$$2 \left[ \nabla \times \left( k(r) \vec{V} \right) \right] - 4 \left( k(r) \omega \right) + 4\lambda \left( \Delta \vec{\omega} \right) = \rho J \frac{D\omega}{Dt} \quad (3)$$

where  $\vec{V}$  is the velocity vector and the micro-rotational vector is  $\vec{\omega}$ . Micro-inertia is denoted by  $J$  and  $\lambda$  is the material constant. Fluid density and fluid pressure are represented by  $\rho$  and  $P$  respectively.  $\mu(r)$  represents the variable blood viscosity, while  $k(r)$  indicates the variable vortex viscosity. Blood is assumed to be incompressible fluid comprising of plasma, suspension of red blood cells, erythrocytes etc. Hematocrit measures the

volume percentage of red blood cells in plasma. Using the fact that the red blood cells are not uniformly dense throughout, the viscosity is assumed to vary in radial direction. To incorporate the variation in dynamic and vortex viscosity, the following equations have been used which are in accordance with the Einstein's equation

$$\mu(r) = \mu_0 \left[ 1 + H \beta \left( 1 - \left( \frac{r}{r_0} \right)^m \right) \right] \quad (4)$$

$$k(r) = k_0 \left[ 1 - H \beta \left( 1 - \left( \frac{r}{r_0} \right)^m \right) \right] \quad (5)$$

where the extreme hematocrit at the center of the artery is  $H$ ,  $\beta$  is a constant having the value 2.5 in case of human blood.  $\mu_0$  is the viscosity of plasma while  $k_0$  is the vortex viscosity in the non-stenotic and non-tapered region. The parameter  $m$  corresponds to the shape of the blood viscosity profile. The shape of the profile given by Eq.(4) is valid only for very dilute suspensions of erythrocytes, and hence is considered to be of parabolic in nature.

The velocity vector ( $\vec{V}$ ) is represented by  $\vec{V} = (u, 0, v)$ , where  $u$  and  $v$  correspond to the radial and the axial velocity components respectively. Micro-rotation vector  $\omega = (0, G, 0)$ .  $u$ ,  $v$  and  $G$  are functions of both  $r$  and  $z$ . The following non-dimensional parameters are introduced

$$\begin{aligned} v' &= v/u_0, \quad u' = uL_1/(\epsilon u_0), \quad k' = k/k_0, \\ j' &= j/r_0^2, \quad p' = p r_0^2/(u_0 \mu_0 L_1), \quad G' = r_0 G/u_0, \\ \zeta' &= \mathbb{L}_1 \zeta/r_0, \quad z' = z/L_1, \quad r' = r/r_0, \quad \mu' = \mu/\mu_0, \quad t' = \Omega t \end{aligned}$$

By introducing the above dimensionless parameters into the component form of the above modelled equations, we obtain the following equations after dropping the prime (i.e, ')

$$\xi \left( \frac{\partial u}{\partial r} + \frac{u}{r} \right) + \frac{\partial v}{\partial z} = 0 \quad (6)$$

$$\begin{aligned} & - 2\delta^2 \frac{N}{1-N} \left( k(r) \frac{\partial G}{\partial z} \right) + \xi \delta^2 \left[ u \frac{\partial^2}{\partial r^2} \left( \mu(r) + \frac{N}{1-N} k(r) \right) + \frac{u}{r} \frac{\partial}{\partial r} \left( \mu(r) + \frac{N}{1-N} k(r) \right) \right] \quad (7) \\ & - \frac{u}{r^2} \left( \mu(r) + \frac{N}{1-N} k(r) \right) + 2 \frac{\partial u}{\partial r} \frac{\partial}{\partial r} \left( \mu(r) + \frac{N}{1-N} k(r) \right) + \frac{1}{r} \left( \mu(r) + \frac{N}{1-N} k(r) \right) \frac{\partial u}{\partial r} \\ & + \left( \mu(r) + \frac{N}{1-N} k(r) \right) \left( \frac{\partial^2 u}{\partial r^2} + \delta^2 \frac{\partial^2 u}{\partial z^2} \right) \\ & = Re \xi \delta^2 \left[ \sigma \frac{\partial u}{\partial t} + \delta \left( \xi u \frac{\partial u}{\partial r} + v \frac{\partial u}{\partial z} \right) \right] + \frac{\partial p}{\partial r} \end{aligned}$$

$$\begin{aligned} & - \frac{\partial p}{\partial z} - 2 \frac{N}{1-N} \left( G \frac{k(r)}{r} + G \frac{\partial k(r)}{\partial r} + k(r) \frac{\partial G}{\partial r} \right) + \left[ v \frac{\partial^2}{\partial r^2} \left( \mu(r) + \frac{N}{1-N} k(r) \right) \right] \quad (8) \\ & + \frac{v}{r} \frac{\partial}{\partial r} \left( \mu(r) + \frac{N}{1-N} k(r) \right) + 2 \frac{\partial v}{\partial r} \frac{\partial}{\partial r} \left( \mu(r) + \frac{N}{1-N} k(r) \right) + \frac{1}{r} \left( \mu(r) + \frac{N}{1-N} k(r) \right) \frac{\partial v}{\partial r} \\ & + \left( \mu(r) + \frac{N}{1-N} k(r) \right) \left( \frac{\partial^2 v}{\partial r^2} + \delta^2 \frac{\partial^2 v}{\partial z^2} \right) \\ & = Re \left[ \sigma \frac{\partial v}{\partial t} + \delta \left( \xi u \frac{\partial v}{\partial r} + v \frac{\partial v}{\partial z} \right) \right] \end{aligned}$$

$$\begin{aligned} & \frac{4(2-N)}{M^2} \left[ \frac{\partial^2 G}{\partial r^2} + \frac{1}{r} \frac{\partial G}{\partial r} - \frac{G}{r^2} + \delta^2 \frac{\partial^2 G}{\partial z^2} \right] - 4k(r)G + 2 \left[ \xi \delta^2 k(r) \frac{\partial u}{\partial z} - v \frac{\partial k}{\partial r} - k(r) \frac{\partial v}{\partial r} \right] \\ & = ReJ \frac{N}{1-N} \left[ \sigma \frac{\partial G}{\partial t} + \delta \left( \xi u \frac{\partial G}{\partial r} + v \frac{\partial G}{\partial z} \right) \right], \end{aligned} \quad (9)$$

where  $Re$  is the Reynolds number and  $\sigma$  is the Strouhal number. The micropolar parameter is denoted by  $M^2 = (r_0^2 k_0 [2\mu_0 + k_0]) / (\gamma [\mu_0 + k_0])$  and  $N = k_0 / (\mu_0 + k_0)$  is the Coupling number. The non-dimensional scaling variables are defined as  $\xi := \epsilon / r_0$  and  $\delta := r_0 / L_1$ .

Here the artery considered for modelling is assumed to be at a distance from the heart and thus it is a low-Reynolds number flow. Under the assumptions of mild stenosis; i.e.,  $\xi (= \epsilon / r_0) \ll 1$  and subject to the additional condition  $\delta (= r_0 / L_1) \approx o(1)$ , we find that  $\frac{\partial p}{\partial r} \ll \frac{\partial p}{\partial z}$  and  $\frac{\partial G}{\partial z} \ll \frac{\partial G}{\partial r}$ . Due to mild stenosis, Eqs.(2.2 - 2.2), get reduced to

$$\frac{\partial v}{\partial z} = 0 \quad (10)$$

$$\frac{\partial p}{\partial r} = 0 \quad (11)$$

$$\begin{aligned} & -\frac{\partial p}{\partial z} - 2 \frac{N}{1-N} \left( G \frac{k(r)}{r} + G \frac{\partial k(r)}{\partial r} + k(r) \frac{\partial G}{\partial r} \right) + \left[ v \frac{\partial^2}{\partial r^2} \left( \mu(r) + \frac{N}{1-N} k(r) \right) \right. \\ & + \frac{v}{r} \frac{\partial}{\partial r} \left( \mu(r) + \frac{N}{1-N} k(r) \right) + 2 \frac{\partial v}{\partial r} \frac{\partial}{\partial r} \left( \mu(r) + \frac{N}{1-N} k(r) \right) + \frac{1}{r} \left( \mu(r) + \frac{N}{1-N} k(r) \right) \frac{\partial v}{\partial r} \\ & \left. + \left( \mu(r) + \frac{N}{1-N} k(r) \right) \frac{\partial^2 v}{\partial r^2} \right] \\ & = Re \sigma \frac{\partial v}{\partial t} \end{aligned} \quad (12)$$

$$-2 \left[ v \frac{\partial k(r)}{\partial r} + k(r) \frac{\partial v}{\partial r} \right] - 4k(r)G + \frac{4(2-N)}{M^2} \left[ \frac{\partial^2 G}{\partial r^2} + \frac{1}{r} \frac{\partial G}{\partial r} - \frac{G}{r^2} \right] = Re J \sigma \frac{N}{1-N} \frac{\partial G}{\partial t} \quad (13)$$

From equation (11), pressure is obtained to be independent of  $r$ . Therefore, the pressure gradient  $\frac{\partial p}{\partial z}$  which appears due to the pumping action of the heart is taken as

$$-\frac{\partial p}{\partial z}(t) = A_0 + A_1 \cos(2\pi f_p t) \quad (14)$$

where  $A_0, A_1$  are the mean and pulsatile components of the pressure gradient of the heart acting along the axis of the tube and  $f_p$  is the pulse frequency.

### 2.3 Boundary conditions

The boundary conditions at the wall of the catheter (i.e. on  $r = r_c$ ) are

$$v = 0 \quad \& \quad G = 0 \quad \text{at} \quad r = r_c \quad (15)$$

When considering microscale fluid flows, several effects become increasingly important, which are typically excluded from the macro-scale fluid flow. One of the effects not included in the classical Navier-Stokes theory is the micro-rotational effects due to rotation of molecules. This is represented using the boundary condition given by

$$G = -\frac{n}{2} \frac{\partial v}{\partial r} \quad \text{at } r = h(z, t), 0 \leq n \leq 1 \quad (16)$$

i.e., the microrotation is same as  $n$  times the fluid vorticity at the interface.

Beavers et al. [3] studied the effect of boundary layer with a slip velocity over a permeable surface on the fluid velocity and his results agreed with the experimental data reasonably well. Further Brunn [5] suggested the likely presence of slip at the wall in case of polar fluids. This is incorporated in the boundary condition

$$\frac{\partial v}{\partial r} = \frac{\gamma}{\sqrt{Da}} \left( u_b + \frac{Da}{\mu(r)|_{\text{arterial wall}}} \frac{\partial p}{\partial z} \right)$$

at  $r = h(z, t)$  where  $L_0 \leq z \leq L_0 + L_1$  (17)

$$v = u_b \text{ at } r = h(z, t) \text{ where } z \leq L_0 \text{ \& } z \geq L_0 + L_1 \quad (18)$$

As per the result obtained by Devanathan et al. [8] the initial velocity is considered as

$$v = 2 \left[ 1 - \frac{r^2}{h(z, t)^2} + \frac{4\alpha}{M^2} I_0(M) \left( \frac{I_0\left(\frac{Mr}{h(z, t)}\right)}{I_0(M)} - 1 \right) \right]$$

\&  $G = 0$  at  $t = 0$  (19)

where  $\gamma$  is a dimensionless quantity depending on the material parameter which characterizes the structure of the permeable material within the boundary region,  $Da$  is the Darcy number,  $u_b$  is the slip parameter,  $M^2$  is the micropolar parameter,  $\alpha = (NM)/(4I_1(M))$  and  $N$  is the coupling number.

### 3 Solution process

#### 3.1 Transformation to the computational domain from the physical domain

The classical exact solutions of the Navier-Stokes equations are valuable in understanding the physical/biological phenomena. It is difficult to get the exact of the modelled problem if it possess the higher order coupled equations. Computational methods based on Finite Differences provide reasonably acceptable solutions.

There are different methods to get the numerical solutions to the blood flow problems. Chakravarty et al. [6] used Runge-Kutta method in their solution procedure. Ismail et al. [11] adopted a finite difference scheme to analyze the governing equations. The use of finite difference method to solve the axisymmetric flow in a complex geometry like a converging-diverging artery is facilitated by the transformation of coordinates. The transformation used to move from the physical domain to the computational domain is given by

$$x = \frac{r - r_c}{h(z, t) - r_c} \quad (20)$$

The transformed governing equations corresponding to Eqs. (11 - 13) are

$$\frac{\partial p}{\partial x} = 0 \quad (21)$$

$$\begin{aligned} & -\frac{\partial p}{\partial z} - \frac{2}{(h(z, t) - r_c)} \frac{N}{1 - N} \left[ G \left( \frac{k(x)(h(z, t) - r_c)}{x(h(z, t) - r_c) + r_c} \right) + G \frac{\partial k(x)}{\partial x} + k(x) \frac{\partial G}{\partial x} \right] \\ & + \frac{1}{(h(z, t) - r_c)^2} \left[ v \frac{\partial^2}{\partial x^2} \left( \mu(x) + \frac{N}{1 - N} k(x) \right) + \frac{v(h(z, t) - r_c)}{x(h(z, t) - r_c) + r_c} \frac{\partial}{\partial x} \left( \mu(x) \right. \right. \\ & \left. \left. + \frac{N}{1 - N} k(x) \right) + 2 \frac{\partial v}{\partial x} \frac{\partial}{\partial x} \left( \mu(x) + \frac{N}{1 - N} k(x) \right) + \frac{h(z, t) - r_c}{z(h(z, t) - r_c) + r_c} \left( \mu(x) \right. \right. \\ & \left. \left. + \frac{N}{1 - N} k(x) \right) \frac{\partial v}{\partial x} + \left( \mu(x) + \frac{N}{1 - N} k(x) \right) \frac{\partial^2 v}{\partial x^2} \right] = Re \sigma \left[ \frac{\partial v}{\partial t} - \frac{x}{(h(z, t) - r_c)} \frac{\partial h}{\partial t} \frac{\partial v}{\partial x} \right] \end{aligned} \quad (22)$$

$$\begin{aligned}
& -\frac{2}{h(z,t)-r_c} \left[ v \frac{\partial k(x)}{\partial x} + k(x) \frac{\partial v}{\partial x} \right] - 4k(x)G + \frac{4(2-N)}{m^2(h(z,t)-r_c)^2} \left[ \frac{\partial^2 G}{\partial x^2} + \frac{h(z,t)-r_c}{x(h(z,t)-r_c)+r_c} \frac{\partial G}{\partial x} \right. \\
& \left. - \frac{(h(z,t)-r_c)^2}{(x(h(z,t)-r_c)+r_c)^2} G \right] = ReJ\sigma \frac{N}{1-N} \left[ \frac{\partial G}{\partial t} - \frac{x}{(h(z,t)-r_c)} \frac{\partial h}{\partial t} \frac{\partial G}{\partial x} \right] \quad (23)
\end{aligned}$$

The transformed boundary conditions corresponding to Eqs.(15 - 18) are

$$v = 0 \quad \& \quad G = 0 \quad \text{at} \quad x = 0. \quad (24)$$

$$G = -\frac{n}{2[h(z,t)-r_c]} \frac{\partial v}{\partial x} \quad \text{at} \quad x = 1 \quad (25)$$

$$\frac{\partial v}{\partial x} = \frac{[h(z,t)-r_c]\gamma}{\sqrt{Da}} \left( u_b + \frac{Da}{\mu} \frac{\partial p}{\partial z} \right) \quad \text{at} \quad x = 1; \quad L_0 \leq z \leq L_0 + L_1 \quad (26)$$

$$v = u_b \quad \text{at} \quad x = 1; \quad z \leq L_0, \quad z \geq L_0 + L_1 \quad (27)$$

and the initial conditions (19) in case of micropolar fluid flow are

$$\begin{aligned}
v = 2 \left[ 1 - \frac{[x(h(z,t)-r_c)+r_c]^2}{h(z,t)^2} \right. \\
\left. + \frac{4M}{\alpha^2} I_0(\alpha) \left( \frac{I_0\left(\frac{\alpha[x(h(z,t)-r_c)+r_c]}{h(z,t)}\right)}{I_0(\alpha)} - 1 \right) \right] \\
\& \quad G = 0 \quad (28)
\end{aligned}$$

### 3.2 Numerical approach

Eqs. (15 - 18) are discretized using finite differences. The difference approximation used for the time derivative is based on a forward difference formula while for the spatial derivatives central difference formula has been used which may be expressed as

$$\begin{aligned}
\left( \frac{\partial v}{\partial t} \right)_{i,j}^k &= \frac{v_{i,j}^{k+1} - v_{i,j}^k}{\Delta t}; \quad \left( \frac{\partial v}{\partial x} \right)_{i,j}^k = \frac{v_{i+1,j}^k - v_{i-1,j}^k}{2\Delta x}; \\
\left( \frac{\partial v}{\partial z} \right)_{i,j}^k &= \frac{v_{i,j+1}^k - v_{i,j-1}^k}{2\Delta z} \quad (29)
\end{aligned}$$

with  $t^k = k\Delta t$ ,  $z_j = j\Delta z$ ,  $x_i = i\Delta x$  and  $v(x, z, t) = v(i\Delta x, j\Delta z, k\Delta t) = v_{i,j}^k$ . Here  $\Delta t$  shows the time step size and  $k$  indicates the time direction.  $\Delta z$  and  $\Delta x$  refer to the length and width of the cell. An explicit time marching procedure is used to simulate the present blood flow model. The solution procedure consists of the following steps:

- Setting up the initial and boundary conditions for the flow variables.
- Calculation of the velocity and the microrotation components from of Eqs. (17 - 18) at the new time step. In the present solver, an explicit time marching technique has been used for this purpose.
- Finally, the physiological parameters, namely volumetric flow, resistance to the flow and shear stress are calculated by using the expressions below

The discretized expressions for the flow rate  $Q_j^k$ , Impedance to the flow  $\Lambda_j^k$ , and shear stress  $(\tau_{rz})_{i,j}^k$  are as follows:

$$Q_j^k = 2 \left( h_j^k - r_c \right) r_c \int_0^1 v_{i,j}^k dx_i + 2 \left( h_j^k - r_c \right)^2 \int_0^1 x_i v_{i,j}^k dx_i \quad (30)$$

$$\Lambda_j^k = \frac{|L(\partial p / \partial z)^k|}{Q_j^k} \quad (31)$$

$$(\tau_{rz})_{i,j}^k = -\frac{N}{1-N} G_{i,j}^k + \frac{1}{h_j^k - r_c} \left( \frac{\partial v}{\partial r} \right)_{i,j}^k. \quad (32)$$

## 4 Results and discussion

The aim of the present work is to study the effects of variable viscosity, arterial wall deformability, catheter size and tapered parameter in addition to the parameters arising out of the fluid and geometry considered, on physiological characteristics of the blood flow. The solutions are obtained for  $\Delta x = \Delta z = 0.025$  and  $\Delta t = 10^{-5}$  with convergence accuracy of the order of  $\approx 10^{-14}$ . The axial velocity profiles, the volumetric flow rate, the resistance to the flow and the wall shear stress are exhibited through their graphical representation by making use of the following parametric values :  $r_0 = 0.152$ ,  $L = 2$ ,  $L_1 = 1$ ,  $L_0 = 0.5$ ,  $u_b = 0.05$ ,  $A_0 = 50$ ,  $A_1 = 0.2A_0$ ,  $f_p = 1.2Hz$ ,  $b = 0.1$ ,  $H = 0.2$ ,  $m = 2$ ,  $\beta = 2.5$ ,  $\gamma = 0.1$ ,  $Re = 10$ ,  $\sigma = 3$ ,  $J = 1$ ,  $M = 10$ ,  $N = 0.5$ .

Table 1: Parameters used for the simulation

Description	Parameter	Value	Reference
Radius of the normal artery	$r_0$	0.152	Bronzino [4]
Variable Viscosity	$\mu(r)$ & $\kappa(r)$	Eqs.(1, 2)	Our study (evident from Bronzino [4])
Fluid parameters	$M$ & $N$	10 & 0.5	Reddy et al. [15]
Pulsatile Pressure Gradient	$\partial p / \partial z$	Eqs.(19)	McDonald [12] & Chakravarty et al. [7]
Arterial segment	$L$	2	Reddy et al. [14]
	$L_1$	1	
	$L_0$	0.5	
Intensity of microrotation	$n$	$0 \leq n \leq 1$	Chakravarty et al. [17]

### 4.1 Velocity profiles

Velocity profiles have been discussed as they provide a detailed description of the flow field. In particular axial velocity component in both the axial and radial directions has been discussed with respect to various parameters.

To validate the present numerical scheme, the results obtained for the axial velocity in case of the Newtonian fluid using the present scheme for non-tapered artery are compared with that of the results obtained by Chakravarty et al. [7]. It has been observed that, the nature of the axial velocity profile is similar in both the cases as shown in Fig. 2, thus validating the scheme. Further the same velocity profile has been considered for micropolar fluid with respect to the initial and boundary conditions of the problem considered. Here it is observed that the magnitude of the velocity is appreciably high in case of micropolar fluid when compared to that of Newtonian fluid. This is highlighting the importance of the consideration of the non-vanishing microrotation and slip velocity at the arterial wall along with the stenosis permeability Figs. (3, 4) give the axial velocity profile for blood flow in the stenotic region of the tapered artery at  $t = 0.85$  at the extreme height locations represented by  $z_L$ ,  $z_C$  and  $z_R$ . Here all the curves in the graph are decreasing from their individual maxima at the wall of the catheter as one moves way from it and eventually it is decreasing in the radial direction. Here it is to be noted that, the velocity never drops down to zero because of the consideration of the slip at the wall



of the artery. Fig. 3 holds the information towards the effect of the tapering angle at different extremes of the stenosis. In general, the tapering in the arteries, pulsatile pressure gradient and pulsatile change in the arterial diameter will facilitate fluid flow. In particular, it is observed that the flow velocity is more in case of diverging tapered artery. It is also worthy to mention that in case of non-tapered artery, flow velocity is maximum at critical height location while at extreme height locations, the velocity is same. In case of divergent and convergent tapered artery the magnitude of the velocity is maximum at  $z_C$ . One may notice that the magnitude of the velocity at  $z_R$  is less than that at  $z_L$  in convergent tapered artery and is having a reverse behavior in case of divergent tapered artery. This effect is attributed to the low Reynolds number considered in the analysis.

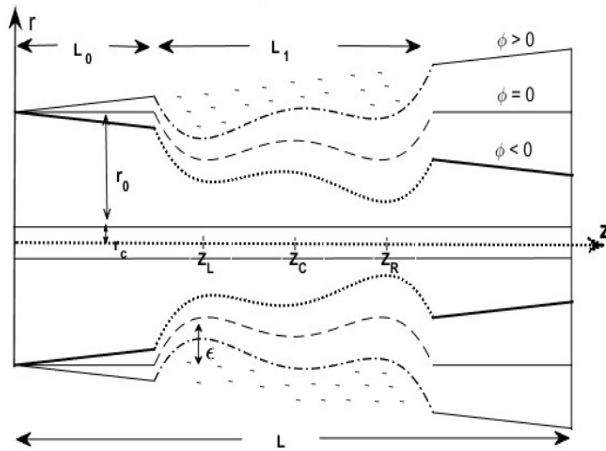


Fig. 1: Schematic diagram of the permeable  $\omega$ -shaped stenotic tapered artery

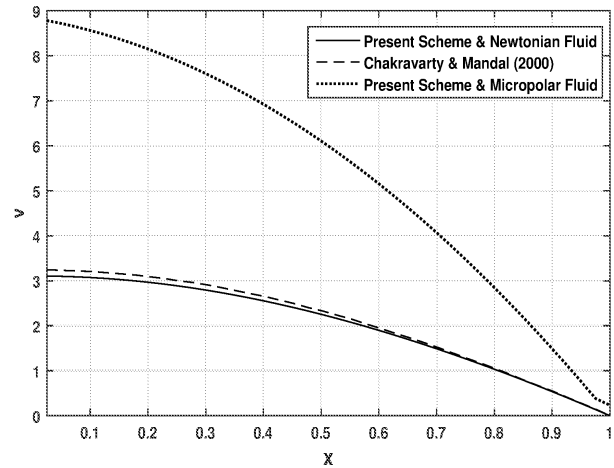


Fig. 2: Axial velocity profile at  $z = 1.0$  and  $\phi = 0^\circ$  for  $t = 0.25$

The influence of the locations of stenosis in the artery on axial velocity for the diverging tapered arterial wall is depicted in Fig. 4. The flow region has been divided into three sections: pre-stenosis (upto  $z = 0.5$ ), stenosis and post-stenosis (from  $z = 1.5$ ). The axial velocity is maximum in non-stenosis region when compared to that of the stenotic region. Fig. 5 illustrates the effect of axial velocity in the axial direction. It is clearly observed that the axial velocity is more in the flow region near the wall of the catheter and it goes on decreasing in the radial direction towards the arterial wall. In case of convergent tapered artery, the difference in magnitudes of the velocities with respect to both the peaks of the stenosis is maximum in main flow and this difference is very less in case of diverging tapered artery. This highlights the importance of studying the vessel tapering effects. The effect of the catheter radius on the axial velocity profile is shown in Fig. 6. It is noticed that the axial velocity and catheter radius are inversely related to each other i.e., as the catheter radius is increasing the axial velocity is decreasing. Further as catheter radius increases the difference in magnitude of the axial velocity with respect to both the peaks is also increasing. It is important to observe that for higher catheter radius, velocity is negative in the vicinity of the second peak. This corresponds to the separation of flow. Further the velocity is minimum at the arterial wall and maximum at the catheter wall for fixed value of the catheter radius.

The micropolar fluid parameter influences the axial velocity at different radial points as shown in Fig. 7. Firstly, it can be noticed that velocity is increasing as micropolar parameter is increasing. This is attributed to the fact that the increase in the micropolar parameter results in the decrease of the coupling effects, thus enabling the fluid to flow with higher velocity. Secondly, at the wall of the artery, the velocity at the stenotic portion is slightly higher and varies for different values of the parameter unlike in the non-stenotic portion, where it is fixed in terms of slip velocity considered on the boundary (Eq.27). Thirdly, reverse flow is observed in post-stenosis region for small value of micropolar parameter. Fig. 8 shows the effect of  $\gamma$ , a parameter which characterizes the permeable material. It is observed that as slip parameter  $\gamma$  increases, the axial velocity at the arterial wall decreases. Further, increase in slip parameter results in sudden decrease in the fluid flow velocity in the post-stenotic region. Hence we see that there is a reverse flow occurring at the offset of the stenosis. More is

the  $\gamma$  value, more is the mismatch in the fluid flow velocities resulting in higher reverse flow. The variation of the axial velocity with respect to the height of the stenosis has been studied in case of diverging tapered artery and is as depicted in the Fig. 9. As the height of the stenosis is increased, the velocity in stenotic region decreases. It is worth observing that in the middle of the flow region, the difference in the magnitude of the axial velocity is maximum for different heights of the stenosis, when compared to that of the other regions. Fig. 10 illustrates the effect of the Darcy number on the fluid flow at stenosed arterial wall. There is no flow across the stenosis in case of Darcy number being zero. Higher the Darcy number enables the fluid to flow more through the stenotic portion thus reducing the velocity at the arterial wall. However, because of this there is more reverse flow occurring after the stenotic portion. This high reverse flow may lead to pathological disorder called aneurysm.

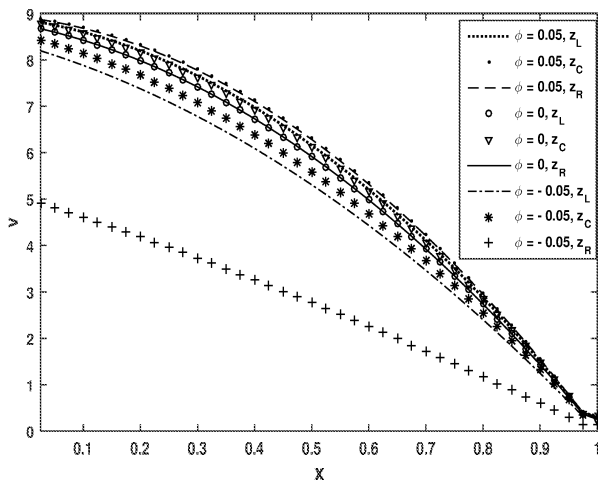


Fig. 3: Axial velocity profile for different  $\phi$  when  $r_c = 0.1, \epsilon = 0.05, n = 1, Da = 0.01$

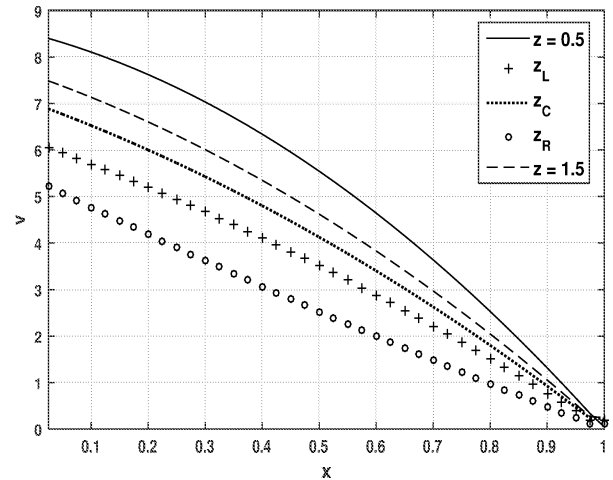


Fig. 4: Axial velocity profile for different axial locations when  $\phi = 0.05, r_c = 0.1, \epsilon = 0.1, n = 1, Da = 0.01$

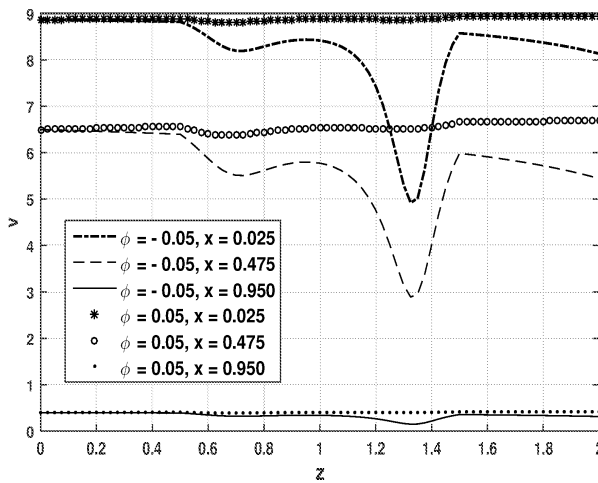


Fig. 5: Axial velocity profile for different radial locations when  $r_c = 0.1, \epsilon = 0.05, n = 1, Da = 0.01$

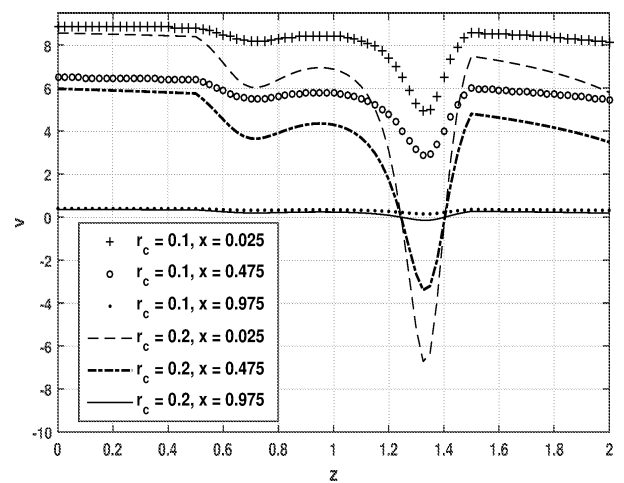


Fig. 6: Axial velocity profile in axial direction for different  $\phi = -0.05, \epsilon = 0.05, n = 1, Da = 0.01$

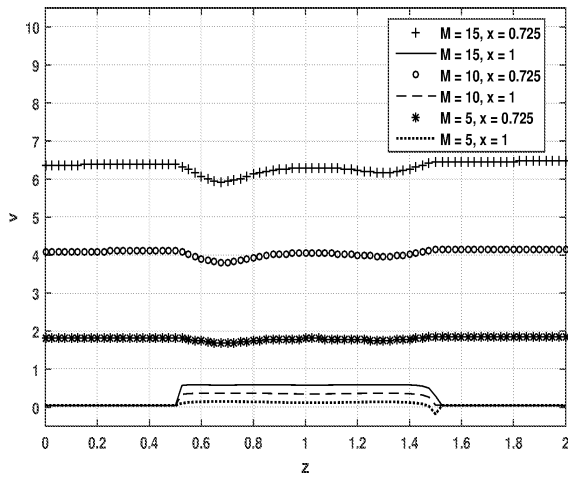


Fig. 7: Axial velocity profile in axial direction for various  $M$  when  $\phi = 0.05, r_c = 0.05, \epsilon = 0.1, n = 1, Da = 0.01$

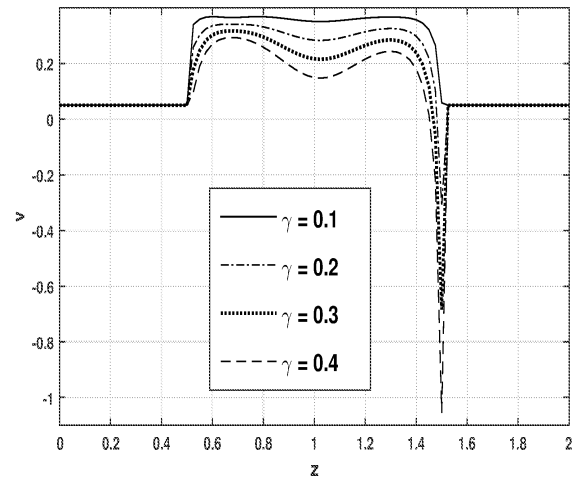


Fig. 8: Axial velocity profile in axial direction for various  $\gamma$  when  $\phi = 0.05, r_c = 0.05, \epsilon = 0.1, n = 1, Da = 0.01$

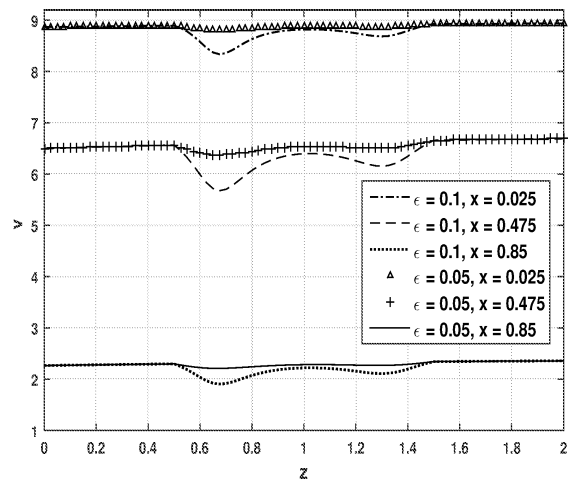


Fig. 9: Axial velocity profile in axial direction for different  $\epsilon$  and  $x$  when  $\phi = 0.05, r_c = 0.1, n = 1, \gamma = 0.1, Da = 0.01$

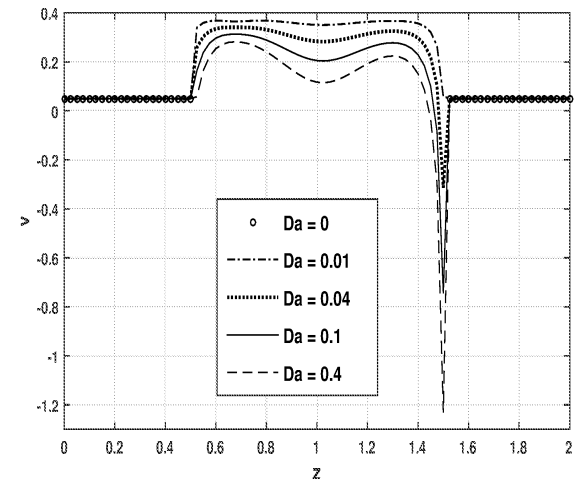


Fig. 10: Axial velocity profile in axial direction for different  $Da$  when  $\phi = 0, r_c = 0.05, \epsilon = 0.1, n = 1, \gamma = 0.1$

### 4.2 Volumetric flow rate

The distribution of the flow rate for different fluid rheology and geometric parameters have also been analyzed. The results are plotted and presented graphically through the Figs. 11-15.

Fig. 11 shows the profile for flow rate in the entire stenotic arterial segment with different taper angles. The volumetric flow rate in the converging tapered artery is more than 2 times less as compared to the flow rate in diverging tapered artery at the second peak. In the non-tapered case, the flow rate is same at both the extremes of the  $\omega$ -shaped stenosis. Here,  $n$  (the proportionality constant related to the micro-rotation vector and the shear stress) = 0 corresponds to the case wherein the particle density is sufficiently great resulting in no-rotation mode of micro-structure elements which are close to the wall. This can be visualized as no micro-rotation at the boundary.  $n = 1$  indicates weak micro-structures concentration, and hence the micro-rotation and angular momentum are equal. As  $n$  is increasing the volumetric flow is increasing and is maximum when the micro-

rotation is same as that of the angular momentum. This is due to high spin of micro-structure elements, which accelerates the flow rate as evident from Fig. 12.

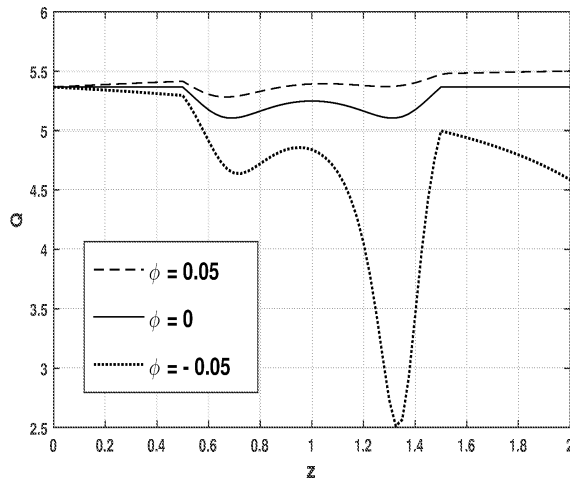


Fig. 11: Variation of volumetric flow rate for various  $\phi$  when  $r_c = 0.1, \epsilon = 0.05, n = 1, Da = 0.1$

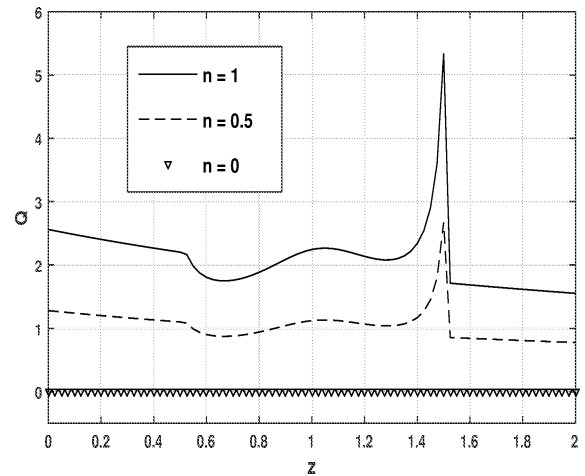


Fig. 12: Variation of volumetric flow rate for various  $n$  when  $r_c = 0.1, \epsilon = 0.05, Da = 0.1$

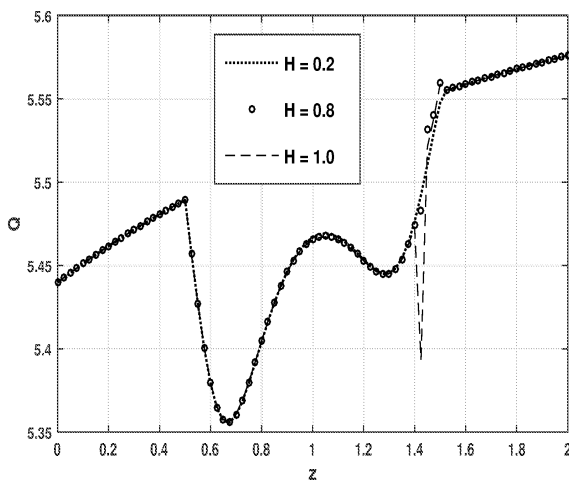


Fig. 13: Variation of volumetric flow rate for different  $H$  when  $\phi = 0.05, r_c = 0.1, \epsilon = 0.05, n = 1, Da = 0.1$

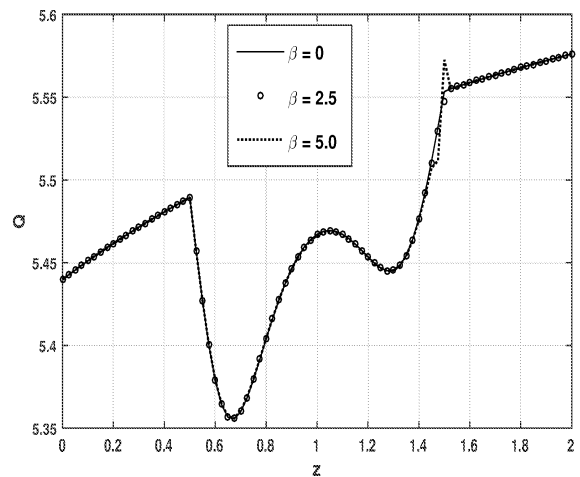


Fig. 14: Variation of volumetric flow rate for different  $\beta$  when  $\phi = 0.05, r_c = 0.1, \epsilon = 0.05, n = 1, Da = 0.1$

The effects of variable dynamic viscosity and vortex viscosity on volumetric flow rate are shown in Figs. 13 - 15. The effects of the hematocrit condition on the flow rate is shown in Fig. 13. From Eq.4 it is observed that the viscosity at the catheter is significantly increasing as  $H$  is increasing. It can be noticed in the figure that the volumetric flow rate is decreasing as  $H$  is increasing. However, it is showing disturbed behavior in the downstream of the stenosis. The increase in viscosity leads to the sudden drop in the volumetric flow rate in the vicinity of the second extremum of the stenosis before stabilizing in the post-stenotic region. The hematocrit constant  $\beta$  is believed to have significant influence on  $Q$ . As  $\beta$  is increasing the flow rate is decreasing. The impact of  $m$  on volumetric flow is depicted in Fig. 15. Here, as  $m$  (the shape of the viscosity profile) is decreasing the shape of the profile is becoming more and more parabolic and viscosity near the arterial wall is decreasing. Therefore the flow rate increases with the decrease of  $m$ .

In all these three figures, the effect is seen mainly in the downstream of the flow.

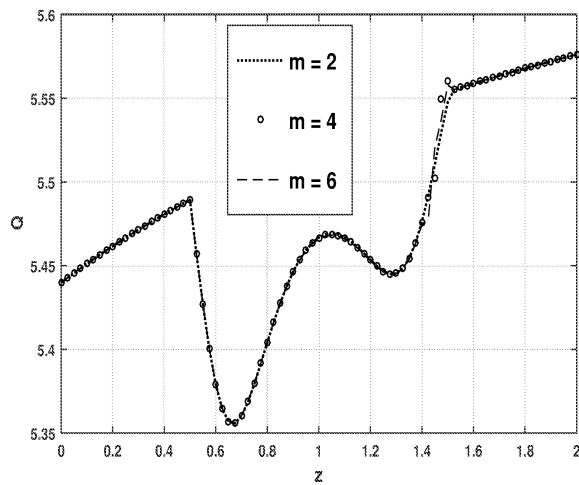


Fig. 15: Variation of volumetric flow rate for different  $m$  when  $\phi = 0.05$ ,  $r_c = 0.1$ ,  $\epsilon = 0.05$ ,  $n = 1$ ,  $Da = 0.1$

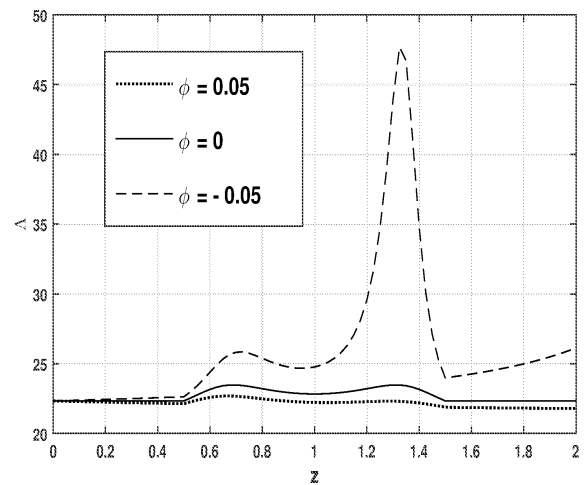


Fig. 16: Variation of the resistance to flow for different  $\phi$  when  $r_c = 0.1$ ,  $\epsilon = 0.05$ ,  $n = 1$ ,  $Da = 0.1$

### 4.3 Resistance to the flow (impedance)

Impedance depends on the flow rate and pressure gradient of the fluid. Hence it is very important to analyze the resistance to the flow. The influence of tapering angle on the impedance ( $\Lambda$ ) is depicted in the Fig. 16. Resistance to flow is more in case of converging artery as compared to non-tapered and diverging tapered artery. The impedance is more at the second extremum of the  $\omega$ -shaped stenosis in converging artery, while it is showing maximum value at the first extrema in case of diverging tapered artery. It is also observed that the resistance to the flow is same at both the extremes in the case of non-tapered artery. The impedance is nearly 2 times higher at the second extrema in case of converging artery as compared to the first extremum, and the variation at extremes is less in case of diverging artery. Figs. 17 - 19 explain the effects of the variable dynamic viscosity and vortex viscosity on the resistance to the flow. The effects of all the three parameters related to variable dynamic viscosity and vortex viscosity are having a similar impact on impedance. In particular, as these parameters increase impedance also increases. As in the case of flow rate, there is disturbed behavior at the downstream of the stenosis, wherein we see a sudden increase in the resistance before coming down and then stabilizing. The sudden drop beyond  $z = 1.4$  upto  $z = 1.5$  could be because of the sudden increase in the annular region.

### 4.4 Shear stress

Shear stress at the wall significantly influences the flow characteristics and rate of mass transfer across the arterial wall. The variation of wall shear stress with different tapering angles is shown in the Fig. 20. The shear stress is same at both the extremes in the case of non-tapered artery. The shear stress is decreasing in case of converging tapered artery and it is increasing in case of diverging tapered artery. The flow velocity is low in case of converging artery, which results in minimum shear stress at the arterial wall. In diverging tapered artery, the shear stress is increasing drastically upto 4 times more in the post-stenosis region. This sudden increase in velocity leads to this variation and may lead to aneurysm. The effect of  $n$  on shear stress is shown in the Fig. 21. It is observed that shear stress is more at the arterial wall when  $n = 0$ . As  $n$  is increasing, the wall shear stress is decreasing. Thus ideally, one would want angular momentum and micro-rotational velocity to match at the boundary for lesser shear stress which would enable artery to be healthy. Finally, in Fig. 22 the effect of the permeable nature of the stenosis is understood on wall shear stress. As observed from the figure, effect of Darcy number is significant only in the stenotic region. It may be observed that the wall shear stress is increasing with

the increase of Darcy number. Therefore, understanding the permeable/non-permeable nature of the stenosis is showing drastic impact on the shear stress.

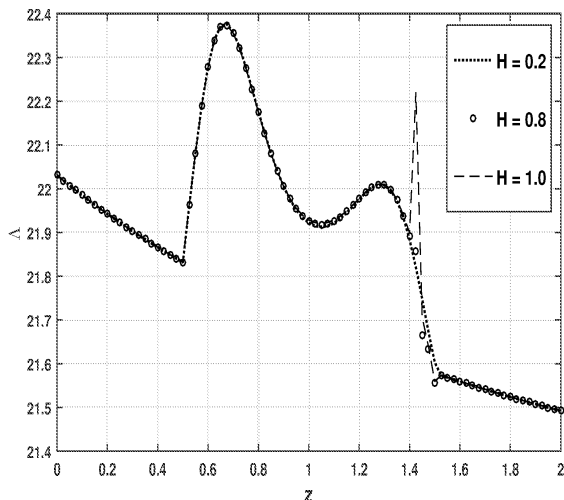


Fig. 17: Variation of the resistance to flow for different  $H$  when  $\phi = 0.05, r_c = 0.1, \epsilon = 0.05, n = 1, Da = 0.1$

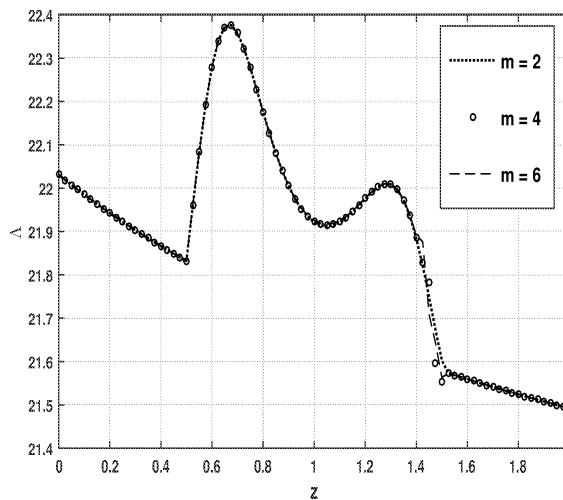


Fig. 18: Variation of the resistance to flow for various  $m$  when  $\phi = 0.05, r_c = 0.1, \epsilon = 0.05, n = 1, Da = 0.1$

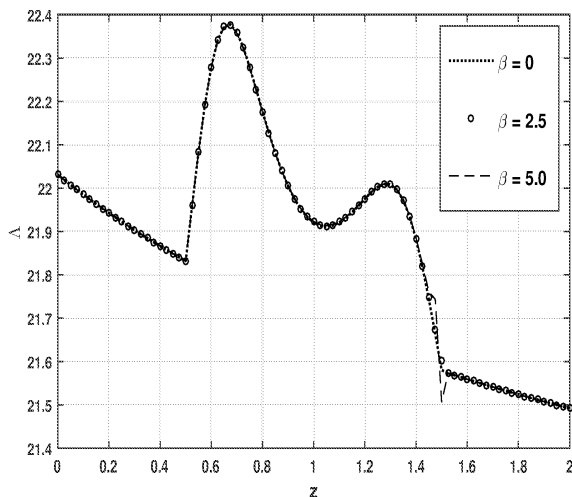


Fig. 19: Variation of the resistance to flow for different  $\beta$  when  $\phi = 0.05, r_c = 0.1, \epsilon = 0.05, n = 1, Da = 0.1$

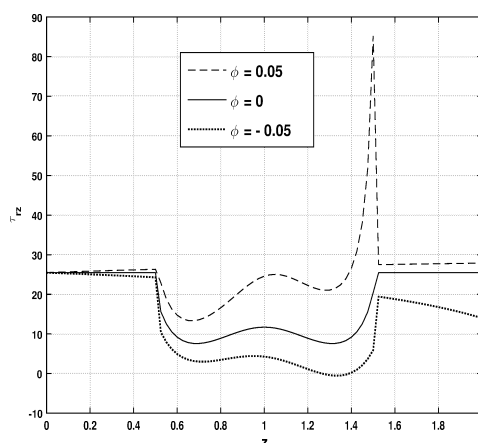


Fig. 20: Variation of the wall shear stress for different  $\phi$  when  $r_c = 0.05, \epsilon = 0.1, n = 1, Da = 0.1$

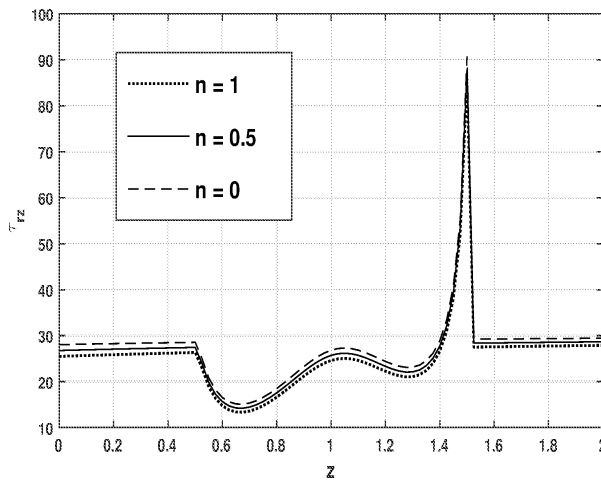


Fig. 21: Variation of the wall shear stress for different  $n$  when  $\phi = 0.05$ ,  $r_c = 0.1$ ,  $\epsilon = 0.05$ ,  $Da = 0.1$

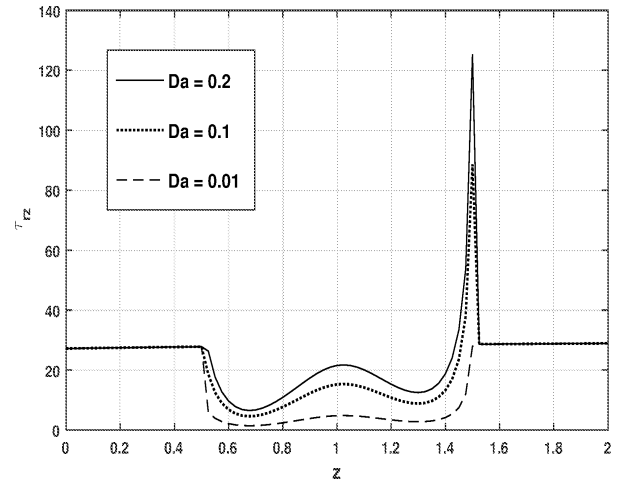


Fig. 22: Variation of the wall shear stress for different  $Da$  when  $\phi = 0$ ,  $r_c = 0.05$ ,  $\epsilon = 0.1$ ,  $n = 1$

## 5 Conclusion

A mathematical model of time dependent blood flow with variable dynamic viscosity and variable vortex viscosity through a tapered artery with  $\omega$ -shaped constriction has been developed. Blood rheology is represented by micropolar fluid, which augments classical laws of continuum mechanics by introducing the effects of fluid molecules on the continuum. Beavers-Joseph ([3]) Darcy boundary condition has been employed at the permeable constricted region. The simulations are carried-out with the finite difference method with desired degree of accuracy. The following are the highlights of the investigation

- A transformation has been used to map the constricted domain into a rectangular one.
- Flow rate is directly proportional to the square of the annular radius. This is because of the low-Reynolds number flow considered in the present discussion.
- It has been observed that there is a negative axial velocity at the arterial wall. Axial velocity decreases as Darcy number and slip parameter increases. It is also observed that there is very high reverse flow at the offset of stenotic portion, and this high reverse flow may lead to the pathological disorder called aneurysm.
- It has been observed that high spin of micro-structure elements accelerates the fluid flow.
- The effects of the parameter related to variable dynamic viscosity and vortex viscosity have significant impact on flow rate and impedance. In particular, as these parameters increases, flow rate decreases and impedance increases.
- Wall shear stress increases as Darcy number increases while the behavior is reversed in the case of the parameter  $n$ .
- It can be concluded that for the artery to be healthy ideally angular momentum and micro-rotational velocity must match at the boundary as this results in lower wall shear stress.

## References

- [1] G. Ahmadi. Self-similar solution of incompressible micropolar boundary layer flow over a semi-infinite plate. *International Journal of Engineering Science*, 1976, **14**(7): 639–646.
- [2] N. S. Akbar. Blood flow suspension in tapered stenosed arteries for walter's b fluid model. *Computer methods and programs in biomedicine*, 2016, **132**: 45–55.
- [3] G. S. Beavers, D. D. Joseph. Boundary conditions at a naturally permeable wall. *Journal of Fluid Mechanics*, 1967, **30**(01): 197–207.

- [4] J. D. Bronzino. *Biomedical engineering handbook*, vol. 2. CRC press, 1999.
- [5] P. Brunn. The velocity slip of polar fluids. *Rheologica Acta*, 1975, **14**(12): 1039–1054.
- [6] S. Chakravarty, A. Datta, P. Mandal. Analysis of nonlinear blood flow in a stenosed flexible artery. *International Journal of Engineering Science*, 1995, **33**(12): 1821–1837.
- [7] S. Chakravarty, P. K. Mandal. Two-dimensional blood flow through tapered arteries under stenotic conditions. *International Journal of Non-Linear Mechanics*, 2000, **35**(5): 779–793.
- [8] R. Devanathan, S. Parvathamma. Flow of micropolar fluid through a tube with stenosis. *Medical and Biological Engineering and Computing*, 1983, **21**(4): 438–445.
- [9] A. C. Eringen. Theory of micropolar fluids. *Tech. Rep.*, DTIC Document, 1965.
- [10] L. Formaggia, A. Quarteroni, A. Veneziani. *Cardiovascular Mathematics: Modeling and simulation of the circulatory system*, vol. 1. Springer Science & Business Media, 2010.
- [11] Z. Ismail, I. Abdullah, N. Mustapha, N. Amin. A power-law model of blood flow through a tapered overlapping stenosed artery. *Applied Mathematics and Computation*, 2008, **195**(2): 669–680.
- [12] D. McDonald. The relation of pulsatile pressure to flow in arteries. *The Journal of Physiology*, 1955, **127**(3): 533 – 552.
- [13] J. R. Reddy, D. Srikanth. The polar fluid model for blood flow through a tapered artery with overlapping stenosis: Effects of catheter and velocity slip. *Applied Bionics and Biomechanics*, 2015, **2015**.
- [14] J. R. Reddy, D. Srikanth, S. K. Murthy. Mathematical modelling of pulsatile flow of blood through catheterized unsymmetric stenosed artery effects of tapering angle and slip velocity. *European Journal of Mechanics-B/Fluids*, 2014, **48**: 236–244.
- [15] J. R. Reddy, D. Srikanth, S. K. Murthy. Mathematical modelling of time dependent flow of non-newtonian fluid through unsymmetric stenotic tapered artery: Effects of catheter and slip velocity. *Meccanica*, 2016, **51**(1): 55–69.
- [16] A. Saini, V. K. Katiyar, M. Parida. Two dimensional model of pulsatile flow of a dusty fluid through a tube with axisymmetric constriction. *World Journal of Modelling and Simulation*, 2016, **12**(1): 70–78.
- [17] Sarifuddina, S. Chakravarty, P. K. Mandal, et al. Heat transfer to micropolar fluid flowing through an irregular arterial constriction. *International Journal of Heat and Mass Transfer*, 2013, **56**(1): 538–551.
- [18] D. Srinivasacharya, G. Madhava Rao. Magnetic effects on pulsatile flow of micropolar fluid through a bifurcated artery. *World Journal of Modelling and Simulation*, 2016, **12**(2): 147–160.
- [19] D. Srinivasacharya, D. Srikanth. Flow of micropolar fluid through catheterized artery - a mathematical model. *International Journal of Biomathematics*, 2012, **5**(02): 1250019.
- [20] V. Srivastava, R. Vishnoi, S. Mishra, P. Sinha. Blood flow through a composite stenosis in catheterized arteries. *ej. Sci. Tech*, 2010, **5**: 55–64.
- [21] W.-T. Wu, N. Aubry, J. F. Antaki, M. Massoudi. Flow of blood in micro-channels: recent results based on mixture theory. *International Journal of Advances in Engineering Sciences and Applied Mathematics*, 2016, 1–11.